Open Access

Propagation of Vector-Meson Spectral-Functions in a BUU Type Transport Model: Application to Di-Electron Production

H.W. Barz[1], B. Kämpfer[1,*], Gy. Wolf[2] and M. Zétényi[2]

[1]*Forschungszentrum Dresden-Rossendorf, Institut für Strahlenphysik, PF 510119, 01314 Dresden, Germany*

[2]*KFKI RMKI, H-1525 Budapest, POB 49, Hungary*

Abstract: The time evolution of vector-meson spectral-functions is studied within a kinetic theory approach. We implement this formalism in a BUU type transport model. Applications focus on ρ and ω mesons being important pieces for the interpretation of the di-electron invariant mass spectrum measured by the HADES collaboration for the reaction C + C at 2 AGeV bombarding energy. Since the evolution of the spectral functions is driven by the local density, the in-medium modifications are tiny for small collision systems within this approach, as the life time of the compressed stage is too short.

Keywords: Heavy-ion collisions, compressed nuclear matter, di-electron emission, broad resonance.

1. INTRODUCTION

Di-electrons serve as direct probes of dense and hot nuclear matter stages during the course of heavy-ion collisions [1-3]. The superposition of various sources, however, requires a deconvolution of the spectra by means of models. Of essential interest are the contributions of the light vector mesons ρ and ω. The spectral functions of both mesons are expected to be modified in a strongly interacting environment in accordance with chiral dynamics, QCD sum rules etc. [1, 2, 4-6]. After the first pioneering experiments with the Dilepton Spectrometer DLS [7, 8] now improved measurements with the High-Acceptance Di-Electron Spectrometer HADES [9-11] start to explore systematically the baryon-dense region accessible in fixed-target heavy-ion experiments at beam energies in the 1 - 2 AGeV region. The invariant mass spectra of di-electrons for the reaction C + C at 1 and 2 AGeV are now available [7, 10, 11] allowing us to hunt for interesting many-body effects.

There are several approaches for describing the emission of real and virtual photons off excited nuclear matter:

(i) A piece of matter at rest in thermal equilibrium at temperature T emits e^+e^- pairs with total momentum q at a rate $dN/d^4xd^4q = -\alpha^2/(3M^2\pi^3) f_B Im\Pi_{em}$ [1, 2], where $f_B(q_0,T)$ is the bosonic thermal distribution function and Π_{em} denotes the retarded electromagnetic current-current correlator, $\Pi_{em} = -i\int d^4x e^{iqx}\Theta(x_0)\langle\langle[j^\mu(x), j_\mu(0)]\rangle\rangle$, the imaginary part of which determines directly the thermal emission rate. Here, α stands for the electromagnetic fine structure constant, M means the invariant mass of the di-electron, j^μ the is electromagnetic current operator, and $\langle\langle\ldots\rangle\rangle$ denotes the ensemble average encoding the dependence on temperature and density (chemical potential), respectively. This rate may be combined with a global dynamic model which provides us the space averaged quantities as a function of time [12] or even adopting a time average [13-16].

(ii) Some sophistication can be achieved by employing a detailed model for the space-time evolution of baryon density and temperature. e.g., as delivered by hydrodynamics. One may also extract from transport models such parameters, where, however, local off-equilibrium and/or anisotropic momentum distributions hamper a reliable definition of density and temperature. Nevertheless, once the rate is given one has a very concise approach, as realized, e.g., in [17]. A similar approach has been presented in [18].

(iii) Microscopic or kinetic transport models do not require isotropic momentum distributions or local equilibrium. Once general principles are implemented, transport models also provide a detailed treatment of the emission of electromagnetic radiation in heavy-ion collisions.

Our approach belongs to item (iii). The time evolution of single particle distribution functions of various hadrons are evaluated within the framework of a kinetic theory. We focus on the vector mesons ρ and ω. The ρ meson is already a broad resonance in vacuum, while the ω meson may acquire a noticeable width in nuclear matter [19]. Therefore, we are forced to treat dynamically these resonances and their decays into di-electrons. Resorting to consider only pole-mass dynamics is clearly insufficient in a microscopic approach [20]. Instead, one has to propagate properly the spectral functions of the ρ and ω mesons. This is the main goal of our paper. We consider our work as being on an explorative level, not yet as a firm and deep theoretically founded prescription of dealing with di-electron emission from excitations with quantum numbers of ρ and ω mesons off excited nuclear matter.

*Address correspondence to this author at the Forschungszentrum Dresden-Rossendorf, Institut für Strahlenphysik, PF 510119, 01314 Dresden, Germany; Tel: +49-351-260-3258; Fax: +49-351-260-3600;
E-mail: b.kaempfer@fzd.de

Our paper is organized as follows. Essential features of our transport model are outlined in section 2. In Subsection 2.1 we describe how the mean field potentials enter in the relativistic transport equation. Subsection 2.2 introduces the dynamics of broad resonances and its implementation in the test-particle method. The crucial quantities for the spectral functions are the self-energies dealt with in subsection 2.3. Subsections 2.4 and 2.5 are devoted to particle production and di-electron emission, respectively. Numerical results of our simulations and a tentative comparison with published HADES data are presented in sections 3 (2 AGeV) and 4 (1 AGeV). Discussion and summary can be found in section 5.

The present analysis supersedes [21], where a first preliminary comparison of transport model results with the C(2 AGeV) + C data [10] has been presented. Further analyses of HADES data have been performed in [22-27].

2. TREATMENT OF HEAVY-ION COLLISIONS

2.1. The Standard BUU Treatment

The employed BRoBUU computer code for heavy-ion collisions developed by a Budapest-Rossendorf cooperation solves a set of coupled Boltzmann-Ühling-Uhlenbeck (BUU) equations in the quasi-particle limit [28, 29]

$$\frac{\partial F_i}{\partial t} + \frac{\partial H}{\partial p}\frac{\partial F_i}{\partial x} - \frac{\partial H}{\partial x}\frac{\partial F_i}{\partial p} = \sum_j C_{ij}, \qquad H = \sqrt{(m_i + U(p,x))^2 + p^2} \tag{1}$$

for the one-body distribution functions $F_i(x,p,t)$ of the various hadron species i, each with rest mass m_i, in a momentum and density dependent mean field U. The scalar mean field U is chosen in such a manner that the Hamiltonian H equals $H = \sqrt{m_i^2 + p^2} + U_i^{nr}$ with a potential U_i^{nr} calculated in the local rest frame as

$$U_i^{nr} = A\frac{n}{n_0} + B\left(\frac{n}{n_0}\right)^{\tau} + C\frac{2}{n_0}\int\frac{d^3p'}{(2\pi)^3}\frac{F_N(x,p')}{1+\left(\frac{p-p'}{\Lambda}\right)^2}, \tag{2}$$

where the parameters A, B, C, τ, Λ define special types of potentials, while n, n_0 and F_N stand for the baryon number density, saturation density and nucleon distribution function. We use the momentum dependent soft potential defined by A=-0.120 GeV, B=0.151 GeV, τ=1.23, C= -0.0645 GeV, Λ=2.167 GeV. The BRoBUU code propagates in the baryon sector the nucleons and 24 Δ and N^* resonances and additionally π,η,σ,ω and ρ mesons. Different particle species are coupled by the collision integral C_{ij} which also contains the Ühling-Uhlenbeck terms responsible for Pauli blocking of spin-1/2 baryons in the collision as well as particle creation and annihilation processes.

The set of coupled BUU equations is solved by using the test-particle method [30-32], where we introduce a number of parallel ensembles. In each ensemble a test particle represents a real particle (nucleon, resonance, pion etc.); collisions happen only within the same ensemble. On the other hand, when calculating such quantities as densities, Pauli blocking factors etc. we average over the ensembles in each time step. This method transforms the partial differential-integro equations (1) into a set of ordinary differential equations (looking like equations of motion) for a number of test particles. A default version of the code has been applied to strangeness dynamics [33-35].

2.2. Off-Shell Transport of Broad Resonances

Recently theoretical progress has been made in describing the in-medium properties of particles starting from the Kadanoff-Baym equations [36] for the Green functions of particles. Applying first-order gradient expansion after a Wigner transformation one arrives at a transport equation for the retarded Green function [37, 38]. In the medium, particles acquire a self-energy $\Sigma(x,p)$ which depends on position and momentum as well as the local properties of the surrounding medium. They have a finite life time which is described by the width Γ related to the imaginary part of the self-energy. Their properties are described by the spectral function being the imaginary part of the retarded propagator $A(p) = -2ImG^{ret}(x,p)$. For bosons the spectral function is related to the self-energy Σ^{ret} *via*

$$A(p) = \frac{\hat{\Gamma}(x,p)}{(E^2 - \vec{p}^{\,2} - m_0^2 - Re\Sigma^{ret}(x,p))^2 + \frac{1}{4}\hat{\Gamma}(x,p)^2}, \tag{3}$$

where the resonance widths Γ and $\hat{\Gamma}$ obey $\hat{\Gamma}(x,p) = -2Im\Sigma^{ret} \approx 2m_0\Gamma$, and m_0 is the vacuum pole mass of the respective particle. The spectral function (3) is normalized as $\int dp^2 A = 2\pi$. (We omit here the label denoting the particle type for simplicity).

To solve numerically the Kadanoff-Baym equations one may exploit the above test-particle ansatz for a modified retarded Green function (see Refs. [37, 38]). This function can be interpreted as a product of particle number density multiplied with the spectral function A. The spectral function can significantly change in the course of the heavy-ion collision process. Therefore, the standard test-particle method, where the test-particle mass is a constant of motion, must be extended by treating the energy $E = p^0$ of the four-momentum p as an independent variable.

Equations of motion for test particles follow from the transport equation. We use the relativistic version of the equations which have been derived in Ref. [37]:

$$\frac{d\vec{x}}{dt} = \frac{1}{1-C}\frac{1}{2E}\left(2\vec{p} + \vec{\partial}_p Re\Sigma^{ret} + \frac{m^2 - m_0^2 - Re\Sigma^{ret}}{\hat{\Gamma}}\vec{\partial}_p\hat{\Gamma}\right), \tag{4}$$

$$\frac{d\vec{p}}{dt} = -\frac{1}{1-C}\frac{1}{2E}\left(\vec{\partial}_x Re\Sigma^{ret} + \frac{m^2 - m_0^2 - Re\Sigma^{ret}}{\hat{\Gamma}}\vec{\partial}_x\hat{\Gamma}\right), \tag{5}$$

$$\frac{dE}{dt} = \frac{1}{1-C}\frac{1}{2E}\left(\partial_t Re\Sigma^{ret} + \frac{m^2 - m_0^2 - Re\Sigma^{ret}}{\hat{\Gamma}}\partial_t\hat{\Gamma}\right), \tag{6}$$

with the renormalization factor

$$C = \frac{1}{2E}\left(\partial_E Re\Sigma^{ret} + \frac{m^2 - m_0^2 - Re\Sigma^{ret}}{\hat{\Gamma}} \partial_E \hat{\Gamma} \right). \quad (7)$$

In the above, $m = \sqrt{E^2 - \vec{p}^2}$ is the mass of an individual test-particle of a given hadron specie. The self-energy Σ^{ret} is considered to be a function of density n, energy E, and momentum $\vec{p}$; thus the dependence on time and position comes only from its density dependence. Partial derivatives with respect to any of the four variables, $t, \vec{x}, E, \vec{p}$, are understood by fixing the three other ones. The quantity $1-C$ has been introduced to ensure that the test particles describe a conserved quantity [38].

The change of the test-particle mass m can be more clearly seen combining Eqs. (5) and (6) to

$$\frac{dm^2}{dt} = \frac{1}{1-C}\left(\frac{d}{dt} Re\Sigma^{ret} + \frac{m^2 - m_0^2 - Re\Sigma^{ret}}{\hat{\Gamma}} \frac{d}{dt}\hat{\Gamma} \right) \quad (8)$$

with the comoving derivative $d/dt \equiv \partial_t + \vec{p}/E\vec{\partial}_x$. This equation means that the square of the particle mass tends to reach a value shifted by the real part of the self-energy within a range of the value of $\hat{\Gamma}$. Thus, the vacuum spectral function is recovered when the particle leaves the medium. This ensures the smooth transition from the in-medium behavior to the vacuum properties, as discussed in detail in [22, 38].

The equation of motions of the test particles have to be supplemented by a collision term which couples the equations for the different particle species. It can be shown [38] that this collision term has the same form as in the standard BUU treatment.

The off-shell transport has been implemented in simulations for the propagation of ρ and ω mesons to study the di-electron productions in γA and pA reactions. Early approaches [39, 40] did not automatically provide the correct asymptotic behavior of the spectral function and an auxiliary potential was introduced to cure this problem. The above equations of motion, which do not have this deficit, were applied to di-electron production in pA collisions in [41] and for AA collisions in [22]. For further developments of transport models we refer the interested reader to [42, 43].

2.3. Self-Energies

To solve the Eqs. (4)-(6) one needs the knowledge of the self-energies. Here one faces the need to decide which effects to take into account in the expression for the retarded self-energy Σ^{ret} in the medium. That is because the BUU transport equations themselves already contain some part of in-medium effects that usually are considered in theoretical models in local density and local equilibrium approximation [44-46]. For instance models for in-medium effects of ρ mesons usually take into account the $N(1520)$-nucleon-hole loop for the self-energy, the corresponding vertices are accounted for in BUU *via* ρ-nucleon scattering and absorption through the $N(1520)$ resonance.

In our calculations we employ a simple schematic form of the self-energy of a vector meson V which accounts for density effects:

$$\mathrm{Re}\Sigma_V^{ret} = 2m_V \Delta m_V \frac{n}{n_0}, \quad (9)$$

$$\mathrm{Im}\Sigma_V^{ret} = m_V (\Gamma_V^{vac} + \frac{nv\sigma_V}{\sqrt{1-v^2}}). \quad (10)$$

(The Lorentz factor in the last equation emerges from the time transformation from the laboratory frame to the comoving frame, since the width corresponds to the lifetime in the eigenframe. At given energies and for the massive vector mesons the velocity v stays sufficiently below unity.) Equation (9) causes a "mass shift" $\Delta m_V = \sqrt{m_V^2 + Re\Sigma_V^{ret}} - m_V$ being roughly proportionally to the density n of the surrounding matter. The imaginary part contains the vacuum width Γ_V^{vac}, the energy dependence of which is described by a form factor [47]. For instance, for $R \to NM$ decays we use the parametrization

$$\Gamma(q) = \Gamma_r \frac{M_r}{M}\left(\frac{q}{q_r}\right)^{2l+1}\left(\frac{q_r^2 + \delta^2}{q^2 + \delta^2}\right)^{l+1}, \quad (11)$$

where l is the angular momentum of the meson, q is the momentum of the meson in the resonance cm system, r index refers to the quantities at the resonance peak and $\delta = 0.3$ GeV. Γ_V^{vac} is accordingly given by Eq. (11) with $l = 1$ for vector mesons.

The second term in Eq. (10) results from the collision broadening which depends on density, relative velocity v and the cross section σ_V of the vector meson in matter. This cross section σ_V is calculated *via* the Breit-Wigner formula

$$\sigma_V = \frac{4\pi}{q_{in}^2}\sum_R \frac{2J_R + 1}{3(2J_V + 1)} \frac{s\Gamma_{V,R}\Gamma_R^{tot}}{(s - m_R^2)^2 + s(\Gamma_R^{tot})^2} \quad (12)$$

for forming resonances with masses m_R, angular momenta J_R, partial widths $\Gamma_{V,R}$, total widths Γ_R^{tot} with energy $\sqrt{s}$ and relative momentum q_{in} in the entrance channel. In vacuum the baryon density n vanishes and the resulting spectral function $A_{vac} = A(n=0)$ is solely determined by the energy dependent width Γ_V^{vac}. We remark that the decay of a test particle is determined by its vacuum width. The life time of a test particle is, furthermore, reduced by the absorption during the two-particle collisions which characterizes the total width $\mathrm{Im}\Sigma_V^{ret}$.

In our actual numerical implementation we assume that the spectral function of the ρ (ω) meson vanishes below two (three) times the pion mass, respectively. (For a discussion of this issue see, for instance, [48]). If a ρ meson is generated at normal nuclear matter density n_0 its mass is distributed in accordance with the spectral function (see Eq. (17) below). If the meson propagates into a region of higher density then the mass will be lowered according to the action of $\mathrm{Re}\Sigma^{ret}$ in Eq. (8). However if the meson comes near the threshold the width $\hat{\Gamma}$ becomes small and the second term of the right hand side of Eq. (8) dominates and reverses this trend leading to an increase of the mass.

The life time of unstable particles is also accessible in the framework of the transport equations for resonances. As it was shown in Ref. [49] this description leads to a life time $\tau = d\delta / dE$, where δ is the energy dependent scattering phase in the formation or the respective decay of the resonance. Although this relation is known for a long time [50] it was introduced only recently in the context of a BUU transport treatment [51]. This prescription is very different from the commonly used formula $\tau = \hbar / \Gamma$. Especially if the resonance is a p wave resonance the life time tends to small values near the threshold in the former case, while it approaches large values in the latter one. If the resonance decays into several channels, the total width is the relevant quantity which describes the phase of the amplitude common to all decay channels:

$$\tan\delta = \frac{-\frac{1}{2}\hat{\Gamma}}{p^2 - m_0^2 - \mathrm{Re}\Sigma^{ret}}. \tag{13}$$

Therefore, the decay rate into a special channel c is given by the partial width $\Gamma_c = b_c \Gamma^{tot}$ according to

$$\tau^{-1} = b_c \Gamma^{tot} = b_c (d\delta / dE)^{-1} \tag{14}$$

with b_c being the branching ratio of the decay into channel c. If we do not mention otherwise, we use the standard prescription for the life time, $\tau = \hbar / \Gamma$, but in some cases we study the effect of using Eq. (14), as well.

2.4. Particle Production

In most instances, a vector meson V is created by the decay of a baryon resonance R in the BRoBUU code. Thus, mesons are created in two-step processes like $NN \leftrightarrow NR$ with subsequent decay $R \leftrightarrow VN$. As mentioned above the BRoBUU model includes 24 non-strange baryon resonances. Their parameters (mass, width and branching ratios) are determined by a global fit to pion-nucleon scattering data, while resonance production cross sections are fitted to inelastic nucleon-nucleon scattering cross sections [47]. Since there are very few $np \to RN$ data we assume that

$$\sigma_{np \to RN} = a \sigma_{pp \to RN}, \tag{15}$$

where a is a channel independent (except one, see below) constant, and its value $a = 1.34$ is obtained from a fit to the few existing data. We use that prescription for all resonances (R) except for N(1535), the main source of η meson, where experimental data indicate a much higher value of $a_{N(1535)} = 5$.

Our approach is in contrast to other ones (e.g. [22, 23]) where individual elementary hadron reaction channels are parameterized independently from one another. Using such a coupled channel approach could allow us to obtain cross sections for not measured or poorly measured channels.

The in-medium spectral functions of ω and ρ mesons also have to be taken into account when their test particles are created. In the resonance decay the mass distribution of the generated test particles for mesons results from an interplay of phase-space effects and the in-medium spectral functions A of the created meson. For the decay of a resonance of mass m_R in a meson of mass m and a baryon of mass m_N we use the phase space distribution in the final state with a constant matrix element squared $|M|^2$

$$\Gamma = N \int d^4 p_N \, \delta(p_N^2 - m_N^2) \int d^4 p_V \frac{1}{2\pi} A(p_V) |M|^2 \tag{16}$$

from which the distribution

$$\frac{dN^{R \to NV}}{dm_V} = N \, m_V \, \lambda^{1/2}(m_R^2, m_N^2, m_V^2) A(m_V) \tag{17}$$

results, where λ is the triangle function $\lambda(a^2, b^2, c^2) = (c^2 - a^2 - b^2)^2 - (2ab)^2$. N is an appropriate normalization factor.

We also include meson emission during a transition $R \to R'V$ from a resonance state R to another resonance R' with $R' = \Delta(1232)$, $N(1440)$, $N(1520)$, $N(1535)$.

In Fig. (**1**) we compare the cross section calculated with our parameter set with data measured by the collaborations

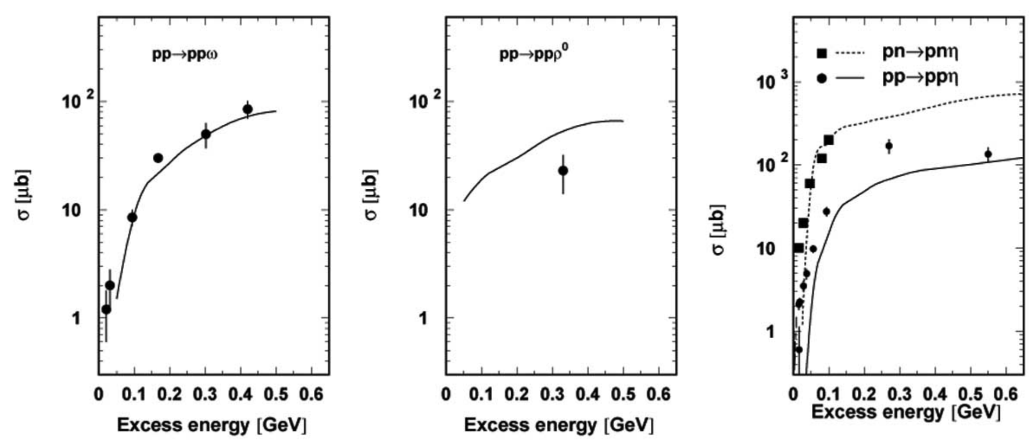

Fig. (1). Production cross sections of ω (left), ρ^0 (middle) and η (right) mesons in pp collisions as a function of the excess energy in comparison with data [52-60].

SATURN, COSY and DISTO [52-60]. The relevant range for collisions in the 1 - 2 AGeV region is at excess energies below 0.5 GeV; very nearby the respective thershold, however, the cross sections are tiny and do not contribute noticeably [61]. We recognize that the ω production in pp collisions is well reproduced by our model parameters. The $pn \to pn\omega$ cross sections are about 1.5 times larger than the pp cross sections. The one-boson exchange model in [62] predicts even a ratio of two.

For the ρ^0 production near threshold there are not many pp measurements. Such measurements are hampered by the large ρ width which make it difficult to discriminate ρ mesons from sequential two pion emission. At an excess energy of 0.33 GeV a ρ^0 cross section of 23 ± 9 μb [56] has been measured, where ρ^0 mesons were identified by pion pairs with masses above 0.6 GeV. The employed global fit including many elementary channels overestimates this cross section by a factor of 2.3. As a consequence we will reduce the ρ production by this factor in the following.

With respect to η production our model describes well the production in pn collision, however it seems to underestimate the production in pp collisions. Since the cross sections in pp collisions are anyhow smaller than those of pn collisions, this fact will not seriously affect our final results.

Furthermore, the ρ mesons can also be created in pion annihilation processes $\pi + \pi \to \rho$ (see below). The dominating channel, however, is $\pi N \leftrightarrow \rho N$ *via* an intermediate resonance R, as mentioned above.

2.5. Di-Electron Production

The di-electron production from direct vector meson decays $V \to e^+e^-$ is calculated by integrating the local decay probabilities along their trajectories in accordance with Eq. (14). The branching ratios b_c of the vector mesons are taken from experimental data at their pole masses. The mass dependence of this branching ratio is assumed to behave proportional to m_V^{-3} in accordance with the vector meson dominance model, where the photon propagator leads to a m_V^{-4} dependence and the phase space of decaying virtual photon modifies this to m_V^{-3}.

The subleading so-called direct channel $\pi\pi \to \rho \to e^+e^-$ is treated with the ρ meson formation cross section

$$\sigma(M) = \frac{\pi}{3p^2} 2m_\rho \Gamma_\rho(p) A_\rho \tag{18}$$

with m_ρ being the actual pole mass of the ρ meson and $\Gamma_\rho(p)$ the vacuum width of the ρ resonance. The in-medium effects are encoded in the spectral function A_ρ.

The ρ meson produces di-electrons with a rate of

$$\frac{dN_{e^+e^-}}{dt} = \left(\frac{m_\rho^0}{m_\rho}\right)^3 b_c \Gamma_\rho(p). \tag{19}$$

We also include into our simulations a bremsstrahlung contribution which is guided by a one-boson exchange model adjusted to pp virtual bremsstrahlung and transferred to pn virtual bremsstrahlung [63]. Actually, we use

$$\frac{d\sigma}{dM} = \frac{\sigma_\perp}{M} \frac{\alpha^2}{6\pi^3} \int \frac{d^3q}{q_0^3} \frac{R_2(\bar{s})}{R_2(s)}. \tag{20}$$

Here M is again the e^+e^- invariant mass, R_2 denotes the two-particle phase space volume, $\sqrt{s}$ stands for the c.m.s. energy; $\bar{s} = s + M^2 - 2q_0\sqrt{s}$ (with q_0 as the di-electron energy in the c.m.s.) is the reduced energy squared after the di-electron emission, and $\sigma_\perp(s)$ is the transverse cross section. Equation (20) can be approximated:

$$\frac{d\sigma}{dM} = \frac{\alpha^2}{3\pi^2} \frac{\sigma_{tot}}{M} \frac{s - (m_1 + m_2)^2}{e_{cm}^2} [\ln(\frac{q_{max} + q_{0max}}{M}) - \frac{q_{max}}{q_{0max}}]. \tag{21}$$

This approximation, employed in [23] too, is applied to pn and πN collisions using the respective corresponding total cross sections σ_{tot}; e_{cm} stands for the energy of the charged particle in the rest system of the colliding particles with masses m$_1$ and m$_2$, $q_{0max} = (s + M^2 - (m_1 + m_2)^2)/2\sqrt{s}$ is the maximum di-electron energy, and $q_{max} = \sqrt{q_{0max}^2 - M^2}$ denotes the maximum di-electron momentum. It should be noted, however, that this cross section is still rather uncertain and needs experimental control.

An essential di-electron contribution comes from the Dalitz decays of π^0, η, ω mesons and the excited baryon resonances emitting a di-electron together with a photon or nucleon. The decay rate Γ_{Dal} for a di-electron of mass M for mesons can quite generally be brought into the form [64].

$$\frac{d\Gamma_{Dal}}{dM} = \frac{4\alpha}{3\pi M} \Gamma_\gamma \left(1 - \frac{M^2}{m_V^2}\right)^3 F(M)^2. \tag{22}$$

The Dalitz decay rates are assumed to be given by the photon partial width Γ_γ which have been taken from experiment [65]. The relevant form factors $F(M)$ for the mesons considered are summarized in [66].

The Dalitz decay of the baryon resonances is treated as in [67]. The most important contribution to the di-electron spectra of these come from the $\Delta(1232)$ resonance. There are also other models [32, 66, 68] for the Dalitz decay. As can be seen on the left panel of Fig. (**2**), these models agree very well for resonance decays from the peak mass, however they differ substantially for Δ resonances with energies (masses) relevant for studying the vector meson region. There is another uncertainty concerning these high-energy (mass) $\Delta(1232)$ resonances. The width and consequently the spectrum of these resonances are sensitive on the cut-off for high masses. Here we show two possible parameterizations (see right panel of Fig. **2**): one from Moniz [69] (solid curve) and the other one from Manley (dotted curve) used in the Particle Data Book [65].

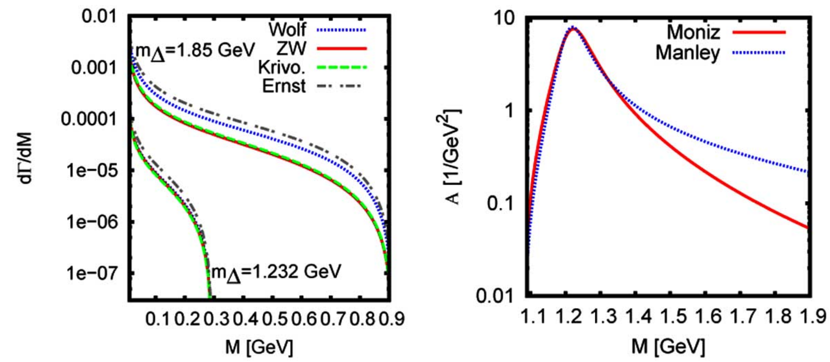

Fig. (2). Left panel: Dalitz- decay of $\Delta(1232)$ for two energies (masses) m_Δ (lower set: 1.232 GeV, upper set: 1.85 GeV) according to the prescriptions [32] ("Wolf"; used, e.g., in [23]), [67] ("ZW"), [68] ("Krivo."; used, e.g., in [24-26]), and [66] ("Ernst", used, e.g., in [22]). Right panel: spectral function with two different cut-off prescriptions according to [69] ("Moniz", solid curve) and [65] ("Manley", dotted curve).

The number of $\Delta(1232)$ resonances at energy (mass) around 1.85 GeV may depend on the cut-off prescription by a factor of 3. Their Dalitz decay (see left of Fig. **2**) panel may differ by a factor of 4. So the Dalitz decay contribution of the $\Delta(1232)$ resonance is uncertain by more than an order of magnitude in the vector meson region. This uncertainty may only be clarified by a detailed comparison of the calculation for $pp \to ppe^+e^-$ with forthcoming experimental data. Using their angular dependence one can localize the different channels and then fix their magnitude. Here we would like to mention that different groups use different prescriptions for that channel which is one reason why the predictions, especially for the $\Delta(1232)$ Dalitz decay contribution, are different. We follow [67] and, accordingly, may somewhat underestimate the di-electron contribution from the Δ channel.

3. RESULTS FOR 2 AGEV

3.1. Spectral Function Dynamics

We employ the above described code for the reaction C(2 AGeV) + C, where data from HADES are at our disposal [10]. In the present explorative study we are going to contrast simulations with and without medium modifications of ρ and ω mesons to elucidate to which degree medium effects may become visible in the light collision system under consideration. In doing so we use fairly schematic medium effects (to be considered as an extreme upper limit) condensed in a "mass shift" described by the above parameter $\Delta m_\omega = -50$ MeV in Eq. (9) for the ω meson. Previous CB-TAPS data [70] suggested indeed such a m_ω mass shift. (See, however, [6] and [71] for a critical discussion of this data). This problem is also investigated experimentally [72] and theoretically [44, 73-75] in calculating the ω spectral function. The use of QCD sum rules [76] then can be utilized to translate this shift into a significantly larger shift for the ρ meson (dictated essentially by the Landau damping term); we use here $\Delta m_\rho = -100$ MeV. We are aware of experiments as reported in Ref. [77-79] which do not observe a noticeable shift of the ρ meson excitation strength. Nevertheless, several theoretical attempts are made to predict a possible ρ "mass shift" during the last decade. Many of them predict a fairly large shift of strength of ρ excitation to lower energy [4, 5], see also [45, 46, 48, 80-83]. Thus, we keep this (presumably too large a) value to illustrate whether it would have a significant imprint on the observed spectra.

Given the present experimental situation [1, 2, 6, 77-79] of not yet having found a solid hint to significant mass shifts we also discuss the option $\Delta m_V = 0$, i.e. collision broadening only.

The spectral function for ρ and ω mesons are shown in Fig. (**3**) at two different densities of nuclear matter and two meson velocities in comparison with the vacuum spectral function. We would like to emphasize the strong velocity dependence of the widths, in particular for the ω mesons.

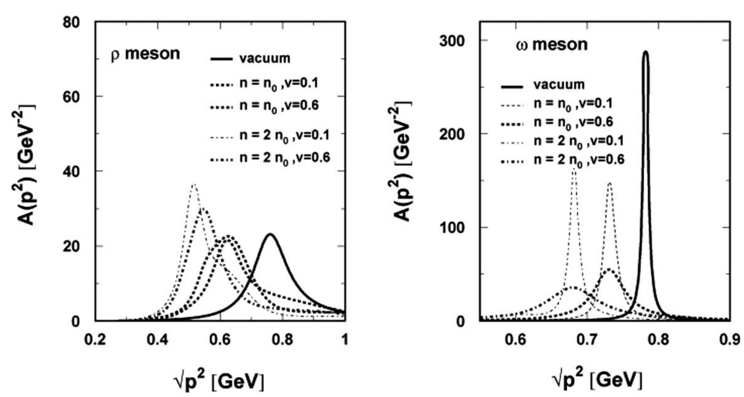

Fig. (3). Influence of medium effects on the spectral functions for ρ (left panel) and ω (right panel) mesons at various nuclear matter densities and velocities in matter.

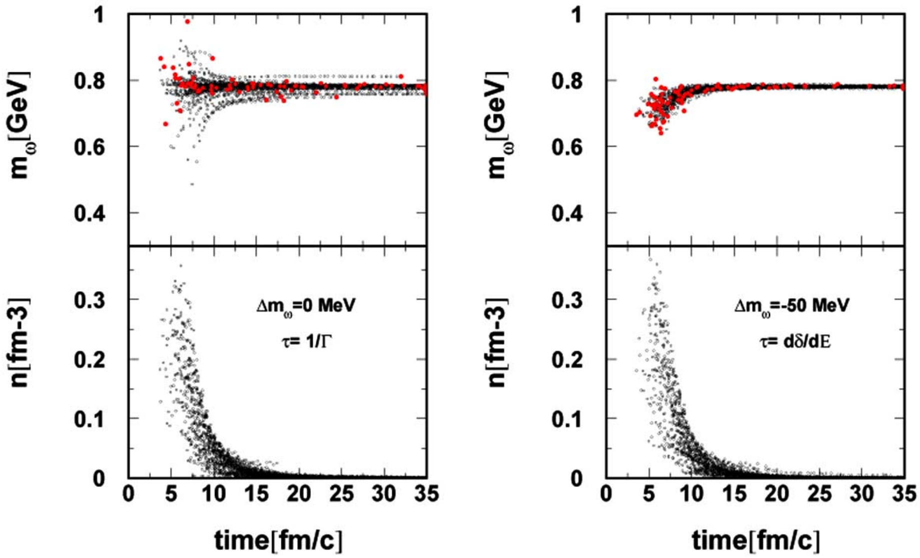

Fig. (4). Time evolution of the masses (upper panels) of about 100 test particles of ω mesons in a C + C collision at 2 AGeV kinetic beam energy at an impact parameter of 1 fm. The red open circles indicate the time instant when test particles are annihilated due to either pionic decay or resonance absorption. The lower part displays the corresponding local densities for the same test particles. The left (without mass shift, i.e. vacuum spectral functions) and right (with mass shift) panels indicate the effect of the spectral function and decay properties.

Despite the excitations of various baryon resonances the spectral functions appear as relatively smooth distributions.

Let us now consider the effect of the mass evolution of the ω and ρ vector mesons given by the equations of motion Eqs. (4)-(6). The ensemble of test particles of mesons is generated in dense matter where their masses are distributed in accordance with their broadened and mass shifted spectral function. In Fig. (**4**) we show the time evolution of a small ensemble of ω test particles. In the calculations the nuclei touch each other at a time of 2.5 fm/c while the density peaks at about 6 fm/c and drops at 8 fm/c below saturation density (see lower part of the figure). At maximum density most of the vector mesons are created, afterwards the mass distribution gets narrower. Only a few of the ω mesons decay in the dense phase where their masses deviate strongly from the pole mass value. If a low density is reached the vacuum spectral function dominates the di-electron decays which leads to a sharp peak at the pole mass. The right hand part of Fig. (**4**) shows the test particles with a spectral function with both the mentioned mass shift and collision broadening, while the distribution on the left hand part is calculated for vacuum spectral functions. Note the apparent squeezing of m_ω for the in-medium case which is caused by the reduced masses since the main decay channel is $\omega \to \rho\pi$, and the ρ's are populating the tail of their distribution.

Fig. (**5**) displays the analog behavior of the test particles of ρ mesons. In the high density stage one recognizes the large spread of the ρ masses of about 300 MeV due to the imaginary part of the self-energy. Most of the ρ mesons decay rapidly (life time $\tau < 2$ fm/c). If we use the relation $\tau = \hbar / \Gamma$ for the life time then essentially the high-mass particles with their large width decay rapidly and, hence, have little chances to radiate di-electrons during their short life time. They look like flashes occurring only in a narrow time interval, thus not causing longer paths of adjacent points in the mass vs. time plot. New mesons are readily created at later times and lower densities. A few low-mass ρ mesons survive these periods and can still be found at 25 fm/c. (In case of $\Delta m_V = 0$ there is no change of the real part of the self-energy. The imaginary part due to collision broadening is small because of the smallness of the cross section for low masses, and its gradient is even smaller. This all together causes only tiny changes of the mass. The same holds for test particles with masses nearby the assumed threshold, where the width goes to zero, see middle panel of Fig. **4**). Therefore, one expects a shift of the di-electron spectra to lower masses. Quite a different picture shows the right hand panel where the life time is calculated accordingly to Eq. (14). Here the low mass particles have a shorter life time than the more massive ones.

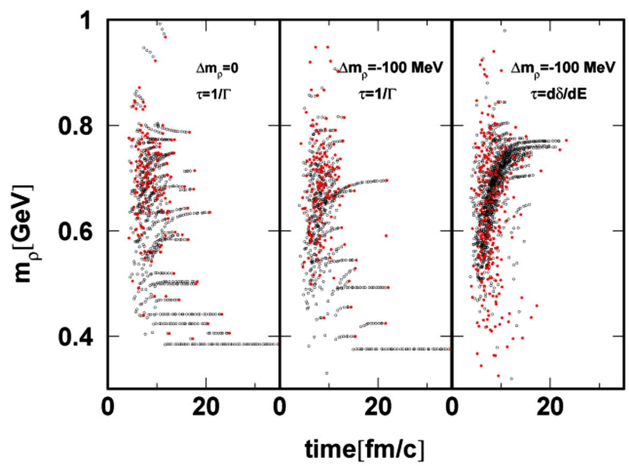

Fig. (5). Time evolution of the masses of about 400 test particles of ρ mesons in a C + C collision at 2 AGeV kinetic beam energy at an impact parameter of 1 fm. The particles in the left panel are calculated with a spectral function without a mass shift while the middle and the right ones the indicated mass shift were used. Note the different prescription for the life time indicated in the legends.

In Fig. (**6**) we exhibit the resulting di-electron spectra from ρ and ω decays for the different prescriptions of the life time. The green dash-dotted curve shows the ρ and ω spectra if the masses of the test particles are kept fixed to the values at the instant of creation. In this case the di-electron spectrum reflects the initial mass distribution which contains the high density spectral function. The effect is best visible for ω mesons near the pole mass: here, the peak at the pole mass would nearly disappear when disregarding the mass evolution. In fact, the sharp ω vacuum peak (red dashed curve) is down shifted and broadened due to averaging over some density interval (cf. Eq. (9)). This is in agreement with the schematic model in [86] for a narrow resonance. However, the time evolution of the off-shell propagation pushes the resulting di-electron spectra towards their vacuum spectral function. If the life time of the vector mesons follows the standard expression $\tau = \hbar / \Gamma$ then the low-mass vector mesons have sufficient time to reach their pole mass. This behavior is also clearly seen (solid curve) for the ω meson. However, if Eq. (14) controls the decay this shift is hindered by an earlier decay of the low mass mesons, see blue dotted curve. The peak position for di-electrons stemming from direct ω decays is nevertheless the same as for a vacuum spectral function. Only for significantly heavier collision systems, which achieve much longer lasting higher maximum compressions, the in-medium modifications may become sizeable (see subsection 3.3).

The direct decays $\rho \to e^+e^-$ reflect to some extent the distribution of ρ excitations: even for a vacuum spectral function a broad distribution emerges. With the assumed strong mass shift, strength is shifted to lower invariant masses, most notably for the life time prescription Eq. (14). Also the "static" scenario (green dash-dotted curve) points to a strong down shift of strength. All together, the various scenarios differ by changes within a factor of two. For heavier collision systems the differences become more pronounced, see subsection 3.3.

Up to now we have contrasted the two extreme scenarios "vacuum" with vacuum spectral functions and "matter" with spectral functions including both the assumed strong mass shifts and the collision broadening. The more realistic option of "collision broadening only" is employed in Fig. (**6**) for two life time prescriptions which cause small differences in the di-electron yields. In what follows we contrast the two extreme scenarios "vacuum" and "matter" which are expected to bracket the realistic case.

Finally we investigate the distribution of the emitted di-electrons as a function of the density of the emitting region.

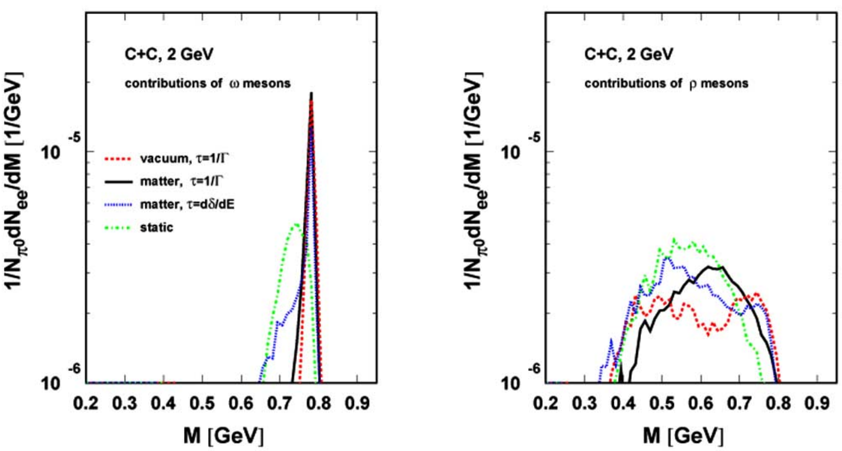

Fig. (6). Di-electron spectra from direct decays of $\omega \to e^+e^-$ (left panel) and $\rho \to e^+e^-$ (right panel) mesons calculated with different assumptions for the dynamics and the spectral functions. "vacuum": vacuum spectral function, "matter": collision broadening and mass shifts with two differen assumption of the life time, "static": in-medium spectral function while the mass evolution of the mesons is switched off.

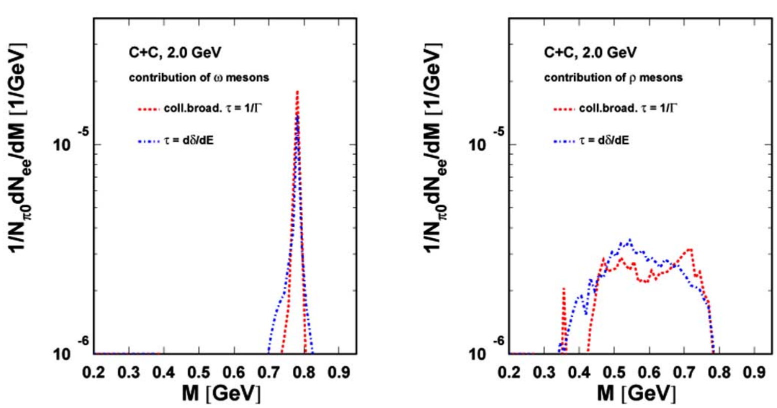

Fig. (7). As Fig. **6** but for collision broadening only. Two life time prescriptions are employed (dashed curves: $\tau = 1/\Gamma$, dot-dashed curves: $\tau = d\delta / dE$).

We consider the effect of the ω mesons in three different density regions: (i) the density $n < n_0 / 3$, (ii) $n_0 / 3 < n < n_0$, and (iii) $n > n_0$. For the light C + C system di-electrons from all regions have similar masses and therefore can be hardly disentangled in experiment, see Fig. (**8**). Let us first consider the scenario with the extreme mass shift of -50 MeV and life time prescription $\tau = \hbar / \Gamma$. The ω peak (blue curve) is determined by e^+e^- stemming from ω decays at density smaller than one third of saturation density (read dashed curve). The contribution from densities between one third and saturation density (green dotted curve) shows clearly the expected mass shift, but its contribution at maximum is less than 10 % of the total yield, i.e. when including the other di-electron sources considered in subsection 3.2. The yield from the high compression stage (red dash-dotted curve) is again a factor of ten smaller.

The situation changes qualitatively for the life time prescription according to Eq. (14), see right panel in Fig. (**8**). However, the down shifted strengths are hidden under the much stronger yields from other sources considered in the next subsection.

3.2. Comparison with HADES Data

While Figs. (**4** – **8**) refer to the central point of our work, we now look at how the evolving ρ and ω spectral functions compare with data. In doing so the other di-electron sources have to be included. The obtained di-electron spectra are represented in Figs. (**9**) and (**10**). In Fig. (**9**) the results exhibited are obtained by including the above described pole-mass shifts as an additional medium modification of ρ and ω mesons. In Fig. (**10**) only the vacuum spectral function is employed. For comparison with the data, the HADES filter has been applied [84] accounting for the geometrical acceptance, momentum cuts and pair kinematics. The filter causes a reduction of the strength and a smearing of the invariant masses of the di-electrons. The result of this filtering is always shown on the right hand panel of the figures.

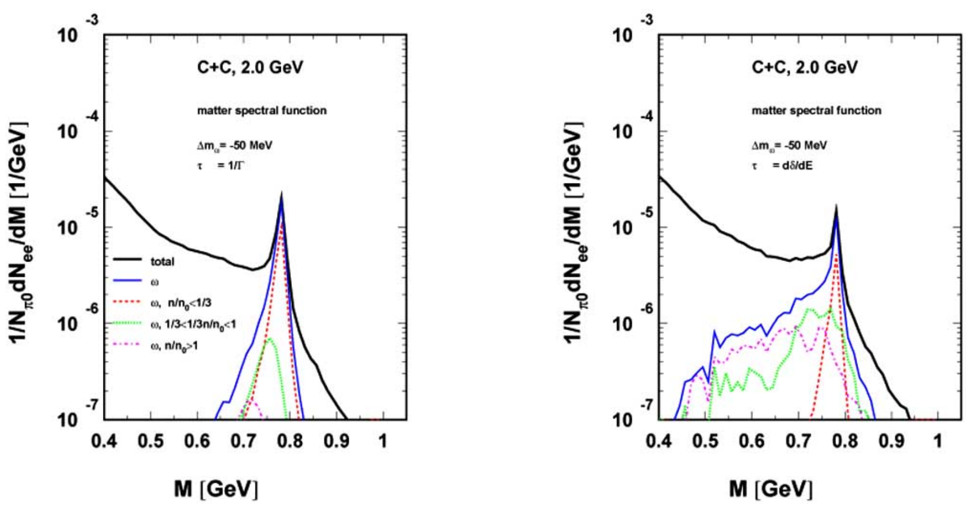

Fig. (8). Contribution to the di-electron yield from ω mesons in various density regions compared with the total yield (thick solid line labelled by "total"). The left picture is calculated with the standard life time for ω mesons, while the right panel shows the effect when using the life time $\tau = d\delta / dE$.

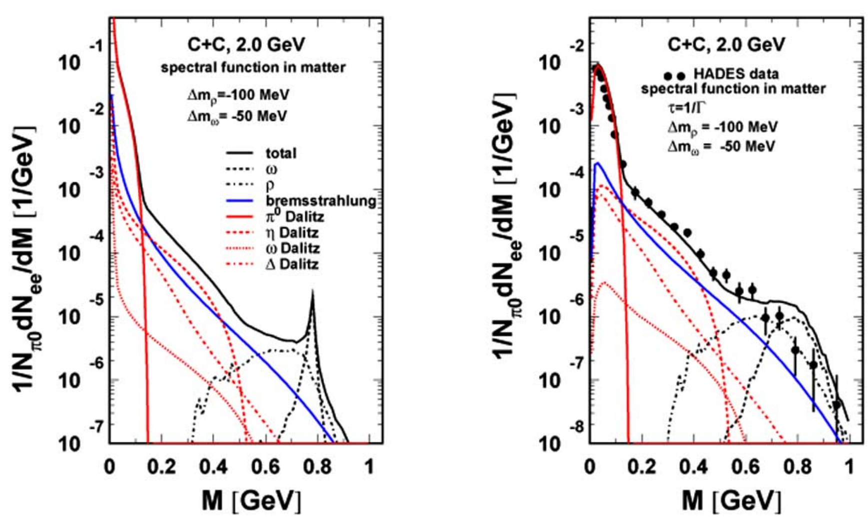

Fig. (9). Di-electron invariant mass spectra for C(2 AGeV) + C calculated with in-medium ("matter") spectral functions. Individual contributions are depicted. Left panel: Full phase space. Right panel: With experimental filter [84] and compared to HADES data, cf. [10] (two data points at very low invariant masses have been discarded).

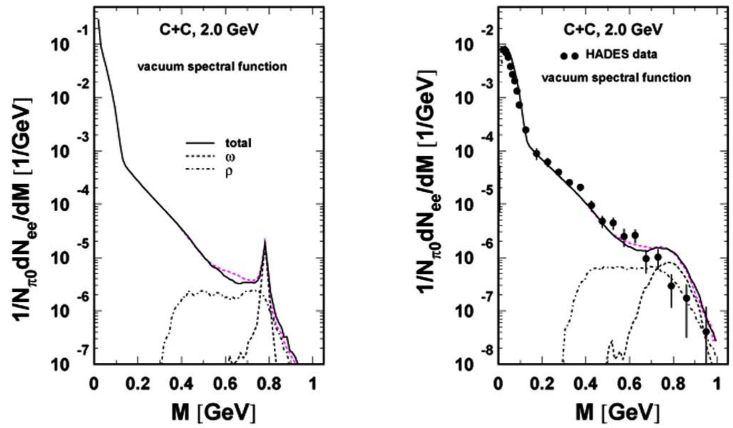

Fig. (10). As Fig. (**9**) but with vacuum spectral functions. The contribution from ω and ρ mesons are indicated. The violett dashed line shows the spectra calculated with the in-medium spectral function from Fig. (**9**).

In these figures we show various contributions to the di-electron rate. Important low-mass di-electron sources are π^0 and η Dalitz decays which are proportional to the multiplicities of their parents. The TAPS collaboration has measured [85] the π^0 and η production cross sections of 707 ± 72 mb and 25 ± 4 mb which have to be compared to our calculations of 870 mb and 23 mb in the same reaction at the same energy. While the values for pion production are overestimated the η production is quite in agreement with the data. (Note that the presently employed cross sections rely on a global fit of many elementary reactions which is not optimized for special channel). The Dalitz decays of ρ and ω mesons and nucleon resonances do not contribute noticeably.

Comparing Figs. (**9**) and (**10**), the mass shifts of the vector mesons do not have a noticeable effect on the overall shape of the di-electron spectra. In particular, the contribution of the cocktail of the other sources mask the effect of the ρ mesons. Furthermore, most of the ω mesons decay outside the dense zone and are therefore not very sensitive for medium effects. Since the fine structure (ω peak) is not yet resolved in the data a conclusive decision cannot be made.

Progress could be made if the di-electron mass resolution is improved to identify the ω peak. However, our calculations do not point to the possibility of a two-peak structure (resulting from a superposition of vacuum decays and in-medium decays) or a substantial smearing of the ω peak due to a density dependent shift analog to the consideration of the ϕ meson (see [86]).

The present set-up provides a reasonable description of the HADES data [9] for di-electron masses below 0.6 GeV. In the higher mass region some overestimation of the data is recognized, as also found in [22, 23, 27]. With respect to the uncertainties of the cross section $pp \to pp\rho$ at threshold and generally the pn channel as well as the role of the resonance channels one could try to improve the agreement by rescaling the ρ and ω contributions. In doing so one could assume unaltered spectral shapes. In fact, agreement with data is achieved by decreasing artificially the cross sections for vector meson production by factors 0.2 for ω and 0.8 for ρ.

The transverse momentum spectra for three invariant mass bins are exhibited in Fig. (**11**). One recognizes a good agreement with these multi-differential data with the exception of the low-p_t region for invariant masses $M > 0.55$ GeV.

3.3. Effects in Larger Collision Systems

The C + C system is rather light and a consequence of it is that the maximum density is about 2.5 n_0 (see Fig. **4**). A heavy system has, in particular, a longer living high-density stage reaching densities of about 3.5 n_0. In Fig. (**12**) we display the result of our calculations for a collision of Au +

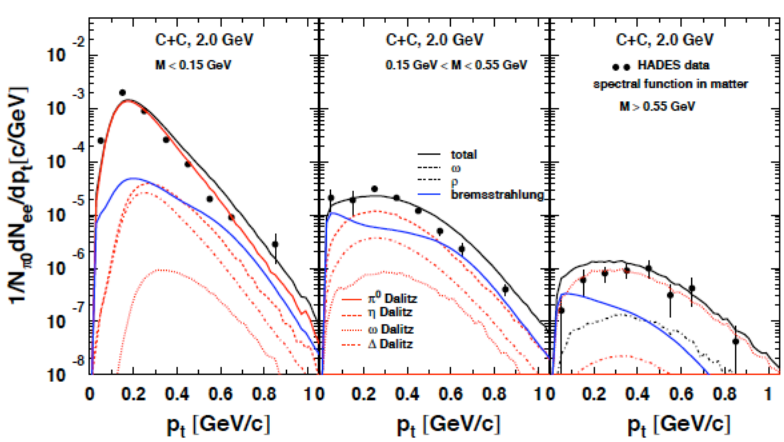

Fig. (11). Transverse momentum spectra for three mass bins. Data source: [87, 88].

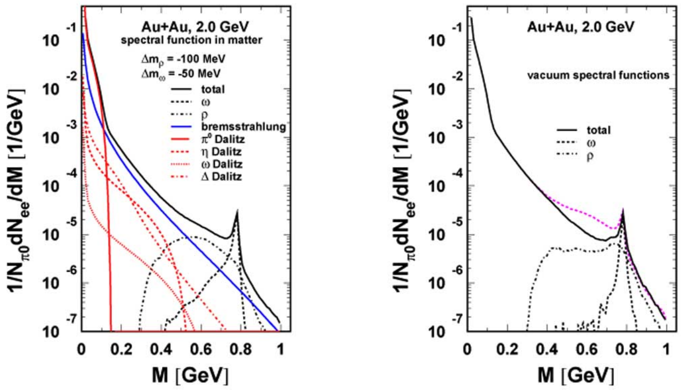

Fig. (12). Di-electron spectra for Au(2 AGeV) + Au. Left panel: In-medium spectral function is used and various contributions to the total spectrum are shown. Right panel: Vacuum spectral function (solid line) in comparison to the spectrum obtained with the in-medium spectral function (dashed violett line).

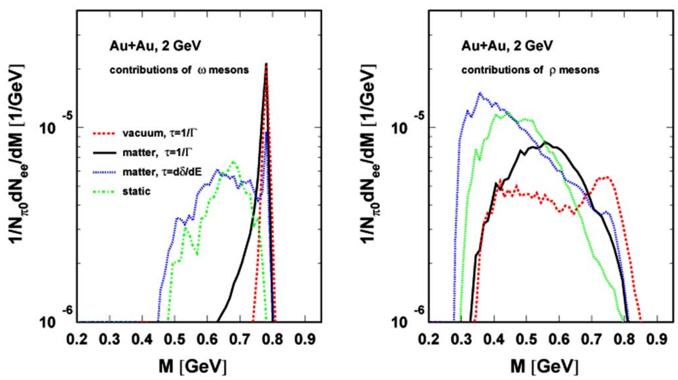

Fig. (13). The same as in Fig. (**6**) but for central Au + Au collisions.

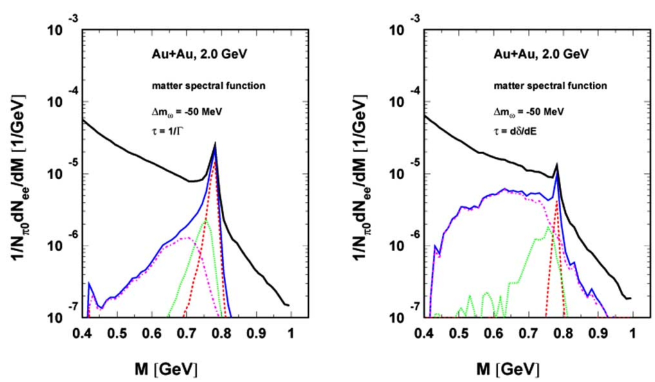

Fig. (14). As in Fig. (**8**) but for the heavy system $Au + Au$.

Au at 2 AGeV. Comparing the left and the right hand part one recognizes the larger effect of the assumed pole mass shifts of the mesons in contrast to the C + C case shown in Figs. (**9**) and (**10**). Furthermore, it is clearly seen that the amount of di-electrons coming from ρ mesons is relatively larger than for light systems. This can be understood by the fact that during the longer collision time ρ mesons can rapidly decay and regenerate

The effects discussed with respect to Fig. (**6**) (life time prescription, vacuum vs. in-medium ("matter") spectral functions, time evolution of spectral functions) are more clearly seen for a larger collision system. Fig. (**13**) shows the dramatic change of the di-electron spectra emitted from ρ and ω mesons in central collisions Au + Au for different assumptions on the spectral functions. The vacuum spectral function of the ρ meson (right panel) still shows the peak near the pole mass despite the m_ρ^{-3} dependence, which causes, together with the ρ excitation, the long flat tail towards the two-pion threshold implemented here. In case of medium modification the shape differs strongly from the vacuum one, with the exception of the standard life time prescription for ω , see left panel in Fig. (**13**).

Repeating the same analysis as in Fig. (**8**) (tracing back the contributions from various density stages) for central Au + Au collisions system we find that ω decay di-electrons from the dense region (red dot-dashed curves) have low masses around 600 MeV and contribute roughly 10% to the total ω yield (see Fig. **14**). There is a remarkable difference between the outcome of the standard life time expression and

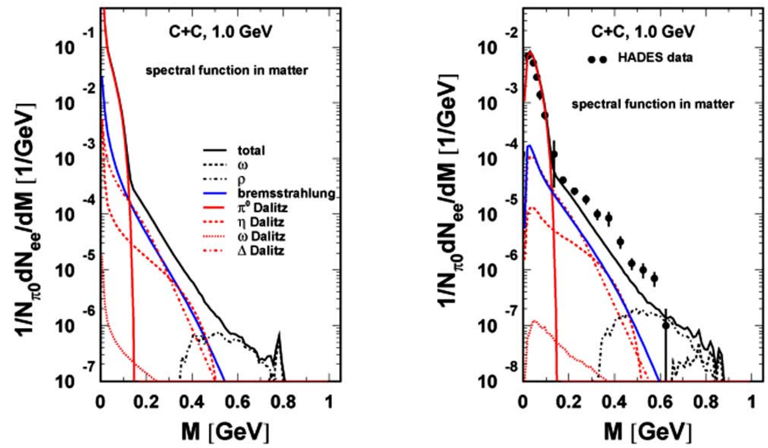

Fig. (15). Di-electron invariant mass spectrum for C(1 AGeV) + C calculated with in-medium spectral functions. Left panel: Spectrum in full phase space. Right panel: Comparison with HADES data [11].

Eq. (14): While for the standard life time prescription the assumed density dependent mass shift is clearly visible (see left panel in Fig. **14**), and the prescription of Eq. (14) causes a strong down shift of strength, reducing eventually the peak height of the ω signal.

4. RESULTS AT 1 AGEV

Recently new HADES data has become available also for C + C collisions at a bombarding energy of 1 GeV per nucleon [11]. The excess energy is about 450 MeV, thus only low energy tails of the ρ and ω mesons play a role. Nevertheless the ρ mesons contribute essentially to the di-electron spectrum above an invariant mass of 500 MeV since other sources are even much smaller, see Figs. (**15**) and (**16**).

We obtain a reasonable agreement with the measured HADES [11] (Fig. **15**) and DLS [7] (Fig. **16**) data, but the data at an invariant mass around 400 MeV are underestimated. The shoulder in the data at 400 MeV could only be explained by a higher contribution of di-electrons coming from the Dalitz decay of the η mesons. We calculate a production cross section $\sigma_\eta = 1.8$ mb which has to be compared to the value $\sigma_{\pi^0} = 450$ mb. The experimental values measured by [85], $\sigma_\eta = 1.5 \pm 0.4$ mb and $\sigma_{\pi^0} = 287 \pm 21$ mb, give a ratio which is a factor of 1.3 larger than our calculated value. Such an increase of the η yield could hardly improve the total di-electron spectra and explain the shoulder at 400 MeV. (It should be noted that a rescaling of π^0 and η contributions in accordance with the TAPS data [85] would result in a better agreement with HADES data [11]). It should be emphasized that, for invariant masses around 350 MeV, the three contributions from η and Δ decays as well as bremsstrahlung are comparable. A strong bremsstrahlung contribution in the pn channel has been advocated in [22] as a convincing solution to the "DLS puzzle". [23] used the same parametrization of bremsstrahlung as we employ here, cf. (21) which in turn is supported by the one-boson exchange model in [63].

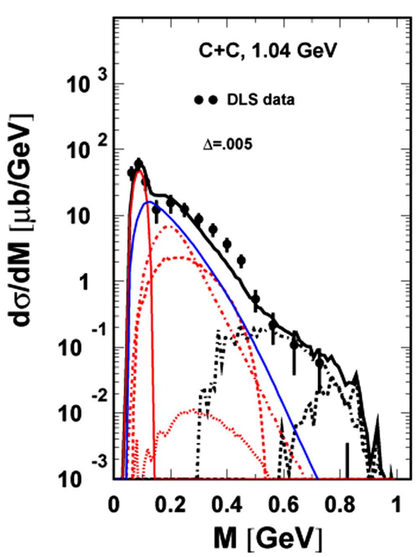

Fig. (16). Comparison of the di-electron spectrum (line codes as in Fig. (**15**)) calculated with the matter spectral functions with the the measurements of the DLS collaboration [7]. The filter described on the DLS web page [89] was used.

Fig. (**17**) exhibits the transverse momentum spectra for three invariant mass bins. A good agreement with available data can be stated. The figure (cf. middle panel) exhibits again the competition of the mentioned three sources with a window at small p_t, where the bremsstrahlung dominates.

5. SUMMARY

In summary we have considered the propagation of broad resonances within a kinetic theory (transport) approach to heavy-ion collisions. Vector mesons are described by spectral functions and these are evolved in space and time by a test-particle method. The motivation for this work is a new generation of data on di-electrons. The corresponding experiments are aimed at seeking imprints of chiral symmetry restoration as particular aspect of in-medium modifications of hadrons. This lets us focus on the treatment of ρ and ω mesons. The wide-spread predictions call for an experimental clarification, but still heavy-ion data need often to be compared with models to extract the wanted information from data.

We have utilized here the transport equations from Ref. [37] which are approximations of the much more involved Kadanoff-Baym equations [93]. Compared to an approach

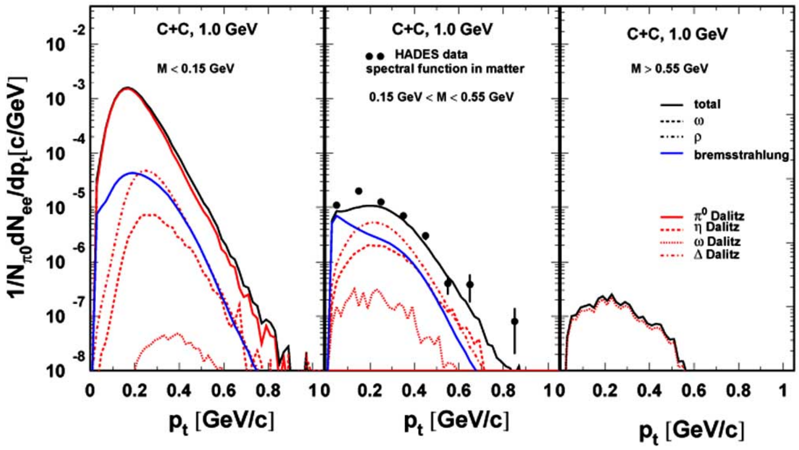

Fig. (17). Transverse momentum spectra for three mass bins at 1 AGeV bombarding energy. Data source: [90-92].

where the spectral function is frozen in after creation the present framework let the spectral functions evolve rapidly towards the vacuum spectral functions. Therefore, the in-medium modifications are washed out, in particular, for the ω meson. In contrast to earlier expectations the ω peak does not suffer a significant modification, even when assuming a strong hypothetical shift of the peak position. Within the employed framework, medium modifications of ρ and ω mesons are hardly seen in the di-electron spectra of small collision systems, even when using fairly strong and schematic assumptions for them. Only heavy collision systems (which achieve somewhat higher compression at a significantly longer time interval) seem to allow us to still identify the wanted medium modifications. The elementary channels which contribute to the overall yields need better control to arrive at firm conclusions on interesting many-body effects.

ACKNOWLEDGEMENTS

We gratefully acknowledge the continuous information by the HADES collaboration, in particular R. Holzmann for delivering and assisting us in using the acceptance filter routines. The work is supported by the German BMBF 06DR136, GSI-FE and the Hungarian OTKA T48833 and T71989.

REFERENCES

[1] Rapp R, Wambach J. Chiral symmetry restoration and dileptons in relativistic heavy ion collisions. Adv Nucl Phys 2000; 25: 1-205.

[2] Rapp R, Wambach J, van Hees H. The chiral restoration transition of QCD and low mass dileptons. Invited review for Landolt-Bornstein 2010, I/23, 4-1. Available from: arXiv:0901.3289.

[3] Tserruya I. Electromagnetic probes. Available from: arXiv: 0903.0415.

[4] Hatsuda T, Lee S-H. QCD sum rules for vector mesons in nuclear medium. Phys Rev 1992; C 46: 34-8.

[5] Brown GE, Rho M. Hadrons in strongly interacting matter. Phys Rept 2002; 363: 85-171. Further references therein.

[6] Leupold S, Metag V, Mosel U. Hadrons in strongly interacting matter. Int J Mod Phys 2010; E 19: 147-224.

[7] Porter RJ, Beedoe S, Bossingham R, *et al.* Dielectron cross-section measurements in nucleus-nucleus reactions at 1 AGeV. Phys Rev Lett 1997; 79: 1229-32.

[8] Wilson WK, Beedoe S, Bossingham R, *et al.* Inclusive dielectron cross-sections in p + p and p + d interactions at beam energies from 1.04 GeV to 4.88 GeV. Phys Rev 1998; C 57: 1865-78.

[9] Salabura P, Agakichiev G, Agodi C, *et al.* Probing of in-medium hadron structure with HADES. Nucl Phys 2005; A 749: 150-9.

[10] Agakichiev G, Dielectron production in ^{12}C + ^{12}C collisions at 2 AGeV with HADES. Phys Rev Lett 2007; 98: 052302-6.

[11] Agakichiev G, Agodi C, Alvarez-Pol H, *et al.* Study of dielectron production in C+C collisions at 1 AGeV. Phys Lett 2008; B 663: 43-8.

[12] Rapp R, Wambach J. Low mass dileptons at the CERN SPS: Evidence for chiral restoration? Eur Phys J 1999; A 6: 415-20.

[13] Kämpfer B, Gallmeister K, Pavlenko OP, Gale C. Dileptons and photons from central heavy ion collisions at CERN SPS. Nucl Phys 2002; A 698: 424-7.

[14] Gallmeister K, Kämpfer B, Pavlenko OP, Gale C. A Unique parametrization of the shapes of secondary dilepton spectra observed in central heavy ion collisions at CERN SPS energies. Nucl Phys 2001; A 688: 939-55.

[15] Gallmeister K, Kämpfer B, Pavlenko OP. A Unique large thermal source of real and virtual photons in the reactions Pb(158 AGeV) + Pb, Au. Phys Rev 2000; C 62: 057901-5.

[16] Gallmeister K, Kämpfer K, Pavlenko OP. Is there a unique thermal source of dileptons in Pb(158 AGeV) + Au, Pb reactions? Phys Lett 2000; B 473: 20-4.

[17] Huovinen P, Belkacem M, Ellis P, Kapusta J. Dileptons and photons from coarse grained microscopic dynamics and hydrodynamics compared to experimental data. Phys Rev 2002; C 66: 014903-12.

[18] Cassing W, Bratkovskaya EL, Rapp R, Wambach J. Probing the rho spectral function in hot and dense nuclear matter by dileptons. Phys Rev 1998; C 57: 916-21.

[19] Wolf Gy, Friman B, Soyeur M. In-medium omega meson broadening and s wave pion annihilation into e+ e- pairs. Nucl Phys 1998; A 640: 129-43.

[20] Knoll J. Transport dynamics of broad resonances. Prog Part Nucl Phys 1999; 42: 177-86.

[21] Barz HW, Kämpfer B, Wolf Gy, Zetenyi M. Propagation of broad meson resonances in a BUU type transport model: Application to di-electron production. Available from: arxiv: nucl-th/0605036v3.

[22] Bratkovskaya EL, Cassing W. Dilepton production and off-shell transport dynamics at SIS energies. Nucl Phys 2008; A 807: 214-50.

[23] Thomere M, Hartnack C, Wolf Gy, Aichelin J. Analysis of dilepton invariant mass spectrum in C + C at 2 AGeV and 1 AGeV. Phys Rev 2007; C 75: 064902-14.

[24] Santini E, Cozma MD, Faessler A, Fuchs C, Krivoruchenko MI, Martemyanov BV. Dilepton production in heavy-ion collisions with in-medium spectral functions of vector mesons. Phys Rev 2008; C 78: 034910-31.

[25] Vogel S, Petersen H, Schmidt K, *et al.* How sensitive are di-leptons from rho mesons to the high baryon density region? Phys Rev 2008; C 78: 044909-17.

[26] Cozma MD, Fuchs C, Santini E, Faessler A. Dilepton production at HADES: Theoretical predictions. Phys Lett 2006; B 640: 170-5.

[27] Schmidt K, Santini E, Vogel S, Sturm C, Bleicher M, Stöcker H. Production and evolution path of dileptons at energies accessible to the HADES detector. Phys Rev 2009; C 79: 064908-23.

[28] Wolf Gy, Cassing W, Mosel U. Eta and dilepton production in heavy ion reactions. Nucl Phys 1993; A 552: 549-70.

[29] Teis S, Cassing W, Effenberger M, Hombach A, Mosel U, Wolf Gy. Pion production in heavy ion collisions at SIS energies. Z Phys 1997; A 356: 421-35.

[30] Wong C-Y. Dynamics of nuclear fluid. VIII. Time-dependent Hartree-Fock approximation from a classical point of view. Phys Rev 1982; C 25: 1460-75.

[31] Bertsch GF, Gupta S. A Guide to microscopic models for intermediate-energy heavy ion collisions. Phys Rep 1988; 160: 189-233.

[32] Wolf Gy, Batko G, Cassing W, Mosel U, Niita K, Schäfer M. Dilepton production in heavy ion collisions. Nucl Phys 1990; A 517: 615-38.

[33] Barz HW, Naumann L. Contribution of the nucleon hyperon reaction channels to K- production in proton nucleus collisions. Phys Rev 2003; C 68: 041901-6.

[34] Barz HW, Zetenyi M, Wolf Gy, Kämpfer B. Subthreshold phi meson production in heavy ion collisions. Nucl Phys 2002; A 705: 223-35.

[35] Barz HW, Zetenyi M. Phi meson production in near threshold proton nucleus collisions. Phys Rev 2004; C 69: 024605-09.

[36] Kadanofff LP, Baym G. Quantum statistical mechanics. New York: Benjamin 1962.

[37] Cassing W, Juchem S. Semiclassical transport of hadrons with dynamical spectral functions in A+A collisions at SIS/AGS energies. Nucl Phys 2000; A 672: 417-45.

[38] Leupold S. Towards a test particle description of transport processes for states with continuous mass spectra. Nucl Phys 2000; A 672: 475-500.

[39] Effenberger M, Bratkovskaya EL, Mosel U. e+ e- pair production from gamma A reactions. Phys Rev 1999; C 60: 044614-28.

[40] Effenberger M, Mosel U. e+ e- pairs from pi-A reactions: Comment. Phys Rev 1999; C 60: 051901-05.

[41] Bratkovskaya EL. e + e- production in pA reactions at SIS energies. Nucl Phys 2001; A 696: 761-87.

[42] Krivoruchenko MI, Fuchs C, Faessler A. Deformation quantization and semiclassical expansion in many-body potential scattering problem. Ann Phys 2007; 16: 587-614.

[43] Krivoruchenko MI, Faessler A. Weyl's symbols of Heisenberg operators of canonical coordinates and momenta as quantum characteristics. J Math Phys 2007; 48: 052107-29.

[44] Lutz M, Wolf Gy, Friman B. Scattering of vector mesons off nucleons. Nucl Phys 2002; A 706: 431-96.

[45] Peters W, Post M, Lenske H, Leupold S, Mosel U. The Spectral function of the rho meson in nuclear matter. Nucl Phys 1998; A 632: 109-27.

[46] Post M, Leupold S, Mosel U. The rho spectral function in a relativistic resonance model. Nucl Phys 2001; A 689: 753-83.

[47] Wolf Gy. Dilepton and vector meson production in heavy-ion reactions. Heavy Ion Phys 1997; 5: 281-97.

[48] Leupold S, Peters W, Mosel U. What QCD sum rules tell about the rho meson. Nucl Phys 1998; A 628: 311-24.

[49] Leupold S. Lifetime of resonances in transport simulations. Nucl Phys 2001; A 695: 377-94.

[50] Baz AI, Zeldovich YaB, Perelomov AM. Rassejanie, reakcii i raspady v nerelativistikoi kvantovoi mekhanike. Moscow: Nauka 1971.

[51] Danielewicz P, Pratt S. Delays associated with elementary processes in nuclear reaction simulations. Phys Rev 1996; C 53: 249-66.

[52] Hibou F, Bing O, Boivin M, *et al.* Near threshold production of omega mesons in the p p $\rightarrow$ p p omega reaction. Phys Rev Lett 1999; 83: 492-5.

[53] Abd El-Samad SM, Abdel-Bary M, Brinkmann KT, *et al.* Production of omega mesons in proton proton collisions. Phys Lett 2001; B 522: 16-21.

[54] Balestra F, Bedfer Y, Bertini R, *et al.* phi and omega meson production in p p reactions at p(lab) = 3.67 GeV/c. Phys Rev 2001; C 63: 024004-18.

[55] Flaminio V, Moorhead WG, Morrison DRO, Rivoire N. Compilation of cross sections III: p and p-bar induced reactions. report CERN-HERA 84-10, 1984.

[56] Balestra F, Bedfer Y, Bertini R, *et al.* rho0 meson production in the p p $\rightarrow$ p p pi+ pi- Reaction at 3.67 GeV/c. Phys Rev Lett 2002; 89: 092001-4.

[57] Calen H, Carius S, Fransson F, *et al.* The p p $\rightarrow$ p p eta reaction near the kinematical threshold. Phys Lett 1996; B 366: 39-43.

[58] Hibou F, Bing O, Boivin M, *et al.* Comparison of eta and eta-prime production in the p p $\rightarrow$ p p eta (eta-prime) reactions near threshold. Phys Lett 1998; B 438: 41-46.

[59] Smyrski J, Wuestner P, Budzanowski A, *et al.* Near threshold eta meson production in proton proton collisions. Phys Lett 2000; B 474: 182-7.

[60] Chiavassa E, Dellacasa G, De Marco N, *et al.* Measurement of the p p $\rightarrow$ p p eta total cross-section between 1.265 GeV and 1.5 GeV. Phys Lett 1994; B 322: 270-4.

[61] Kolomeitsev EE, Hartnack C, Barz HW, *et al.* Transport theories for heavy ion collisions in the 1 AGeV regime. J Phys 2005; G 31: S741-58.

[62] Kaptari LP, Kämpfer B. Combined analysis of near-threshold production of omega and phi mesons in nucleon-nucleon collisions within an effective meson-nucleon model. Eur Phys J 2005; A 23: 291-304.

[63] Kaptari LP, Kämpfer B. Di-electron bremsstrahlung in intermediate-energy pn and Dp collisions. Nucl Phys 2006; A 764: 338-370, Di-clectrons from resonances in nucleon-nucleon collisions. Phys Rev 2009; C 80: 064003-15.

[64] Lautrup BE, Smith J. Radiative corrections to decays with a Dalitz pair. Phys Rev 1971; D 3: 1122-35.

[65] Groom DE, Aguilar-Benitez M, Amsler C, *et al.* Review of particle physics. Eur Phys J 2000; C 15: 1-878.

[66] Ernst C, Bass SA, Belkacem M, Stöcker H, Greiner W. Intermediate mass excess of dilepton production in heavy ion collisions at BEVALAC energies. Phys Rev 1998; C 58: 447-56.

[67] Zétényi M, Wolf Gy. Baryonic contributions to the dilepton spectrum of nucleon-nucleon collisions. Phys Rev 2003; C 67: 044002-9.

[68] Krivoruchenko MI, Martemyanov BV, Faessler A, Fuchs C. Electromagnetic transition form-factors and dilepton decay rates of nucleon resonances. Ann Phys 2002; 296: 299-346.

[69] Koch JH, Moniz EJ, Ohtsuka N. Nuclear photoabsorption and Compton scttering at intermediate energies. Ann Phys 1984; 154: 99-160.

[70] Trnka D, Anton G, Bacelar JCS, *et al.* First observation of in-medium modifications of the omega meson. Phys Rev Lett 2005; 94: 192303-6.

[71] Kaskulov M, Hernandez E, Oset E. Inclusive omega photoproduction from nuclei and omega in the nuclear medium. Eur Phys J 2007; A 31: 245-54.

[72] Naruki M, Funahashi H, Fukao Y, *et al.* Experimental signature of the medium modification for rho and omega mesons in 12 GeV p + A reactions. Phys Rev Lett 2006; 96: 092301-4.

[73] Martell AT, Ellis PJ. Properties of the omega meson at finite temperature and density. Phys Rev 2004; C 69: 065206-11.

[74] Steinmueller B, Leupold S. Weighted finite energy sum rules for the omega meson in nuclear matter. Nucl Phys 2006; A 778: 195-216.

[75] Muehlich P, Shklyar V, Leupold S, Mosel U, Post M. The Spectral function of the omega meson in nuclear matter from a coupled-channel resonance model. Nucl Phys 2006; A 780: 187-205.

[76] Thomas R, Zschocke S, Kämpfer B. Evidence for in-medium changes of four-quark condensates. Phys Rev Lett 2005; 95: 232301-4.

[77] Wood MH, Djalali C, Nasseripour R, *et al.* Medium modifications of light vector mesons in photoproduction reactions at Jlab. Int J Mod Phys 2009; A 24: 309-16.

[78] Wood MH, Nasseripour R, Weygand DP, *et al.* Light vector mesons in the nuclear medium. Phys Rev 2008; C 78: 015201-15.

[79] Nasseripour R, Wood MH, Djalali C, *et al.* Search for medium modification of the rho meson. Phys Rev Lett 2007; 99: 262302-5.

[80] Harada M, Sasaki C. Dropping rho and a(1) meson masses at chiral phase transition in the generalized hidden local symmetry. Phys Rev 2006; D 73: 036001-15.

[81] Ruppert J, Renk T, Müller B. Mass and width of the rho meson in a nuclear medium from Brown-Rho scaling and QCD sum rules. Phys Rev 2006; C 73: 034907-12.

[82] Leupold S. Rho meson properties from combining QCD based models. Nucl Phys 2004; A 743: 283-302.

[83] Cabrera D. Chiral unitary approach to the rho meson in the nuclear medium. Nucl Phys 2003; A 721: 759-62.

[84] Holzmann R. (HADES Collaboration), priv. communiction on the HADES filter HAFT 2006.

[85] Averbeck R, Doeppenschmidt A, Appenheimer M, *et al.* Production of pi0 and eta mesons in carbon-induced relativistic heavy ion collisions. Z Phys 1997; A 359: 65-73.

[86] Kämpfer B, Pavlenko OP, Zschocke S. Dilepton production from hot hadronic matter in nonequilibrium. Eur Phys J 2003; A 17: 83-7.

[87] Eberl T. Di-electron production in C + C and p + p collisions with HADES. Eur Phys J 2007; C 49: 261-7.

[88] Sudol M. Measurement of low-mass e+e- p pair production in 2 AGeV C-C collisions with HADES. PhD dissertation, JWG University Frankfurt 2007.

[89] DLS filter. Available from: http://macdls.lbl.gov/DLS_WWW_Files/AA_Letter/AA.html

[90] Pachmayer Y, Agakichiev G, Agodi C, *et al.* Dielectron production in C+ C collisions at 1 AGeV and the solution to the DLS Puzzle. J Phys 2008; G 35: 104159-65.

[91] Sudol M, Agakishiev G, Agodi C, *et al.* Measurement of low-mass e+ e- pair production in 1 AGeV and 2 AGeV C+C collision with HADES. Eur Phys J 2009; C 62: 81-4.

[92] Pachmayer Y. Dielektronenproduktion in C + C Kollisionen bei 1 GeV pro Nukleon. PhD dissertation, JWG University Frankfurt 2008.

[93] Schenke B, Greiner C. Dilepton production from hot hadronic matter in nonequilibrium. Phys Rev 2006; C 73: 034909-27.

Received: October 08, 2009 Revised: July 23, 2010 Accepted: August 04, 2010